Proceedings of the ASME 2022 17th International Manufacturing Science and Engineering Conference
MSEC2022
June 27-July 1, 2022, West Lafayette, Indiana, USA

MSEC2022- XXXXX

ANALYSIS OF CONDUCTION COOLING STRATEGIES FOR WIRE ARC ADDITIVE MANUFACTURING

Lauren Heinrich[1]
Georgia Institute of Technology
Atlanta, GA

Thomas Feldhausen
Oak Ridge National Laboratory
Manufacturing Science Division
Oak Ridge, TN

Kyle S. Saleeby
Oak Ridge National Laboratory
Manufacturing Science Division
Oak Ridge, TN

Christopher Saldana
Georgia Institute of Technology
Atlanta, GA

Thomas R. Kurfess
Oak Ridge National Laboratory
Manufacturing Science Division
Oak Ridge, TN

ABSTRACT

Metal additive manufacturing (AM) processing consists of numerous parameters which take time to optimize for various geometries. One aspect of the metal AM process that continues to be explored is the control of thermal energy accumulation during component manufacturing due to the melting and solidification of the feedstock. Excessive energy accumulation causes thermal failure of the component while minimal energy accumulation causes lack of fusion with the build plate or previous layer. The ability to simulate the thermal response of an AM component can increase research efficiency by reducing the time to optimize thermal energy accumulation. This paper presents an effective implementation of finite element analysis to determine the thermal response of a wire arc additive manufactured component with various build plate sizes and cooling methods including, integral build plate cooling, oversized build plates with passive cooling, and non-integral build plate cooling. The use of integral build plate cooling channels was shown to decrease the interpass temperature at the conclusion of the build process by 55% and build plate temperature by 96% compared to the conventionally deposited sample with 20 second dwell time. The use of a tall build plate with passive cooling was shown to reduce the interpass temperature by 32% as compared to the conventionally deposited sample with 20 second dwell time. Each cooling strategy evaluated decreased the interpass temperature within a range of 20-55% which enables higher deposition rates and decreased dwell times during depositions. The cooling strategies are designed to be implemented in a hybrid or retrofit AM platform to mitigate concerns of the thermal input from the additive process having detrimental effects on the precision of the machining process. This paper shows that accurate simulations of all strategies can be used to accurately predict the thermal response of the various strategies discussed. These cooling strategies will allow for increased deposition rates with comparable interpass temperature and decreased dwell time, increasing deposition efficiency. These simulations are verified by experimental results. It is concluded that passive strategies, such as the over-sized tall build plate, can be used when liquid coolant in the AM environment could negatively affect the deposition process. Active cooling strategies, such as the integral build plate cooling could be used if low thermal conductivity materials are deposited or higher material deposition rates are desired. This paper discusses the use of active and passive cooling used during AM and shows how a simulation model can be used to make design choices for cooling strategies. The model also enables verification of select critical process parameters such as dwell times for a desired interpass temperature.

[1] Contact author: lheinrich6@gatech.edu

Keywords: Hybrid Manufacturing, Retrofit Additive Manufacturing, Finite Element Analysis, Wire Arc Additive Manufacturing

1. INTRODUCTION

Additive manufacturing (AM) is profitable for high buy-to-fly components, and AM development includes goals of achieve higher efficiencies [1]. Aerospace component high buy-to-fly manufacturing costs boost the development of additive manufacturing techniques for thin walled structures and high-performance materials, such as 6Al-4V titanium [2]. Wire arc additive manufacturing (WAAM) is often more affordable than powder AM systems and is capable of higher material output than many powder-based systems [1,3]. High material output systems can be difficult to optimize the material deposition rate versus a required dwell time in order to achieve an optimal interpass temperature throughout the AM process. Specifically, WAAM process efficiency is low for medium components due to required cooling time in order to prevent structural failure [4]. Thermal structural failure occurs when greater amounts of thermal energy is added to the system than the thermal energy dissipation rate. The energy accumulation causes the melt pool solidification time to increase. As the melt pool solidification time increases, gravity has a more significant effect, decreasing the bead height [5]. Under extreme circumstances, molten feed stock material will flow from the deposition location [4]. Researchers have evaluated various cooling techniques including thermoelectric conduction cooling [6], cold air cooling [7], nozzle and build plate cooling [8], and liquid cooling through component submersion[9]. The analysis of the effectiveness of each cooling method achieved increased bead geometry refinement throughout the duration of the build and decreased dwell time supporting that applied cooling can increase component quality[6–9]. Dinovitzer et al. [1] evaluated the effect of reducing energy input for successive layers of a WAAM wall and successfully decreased bead width in upper deposited layers of a single bead wall. The decreased width indicates faster weld pool solidification and less thermal energy accumulation [5]. Each evaluation described successfully increased efficiency by decreasing dwell time and increasing material efficiency. However, cooling also creates large thermal gradients between the deposition location and cooling location increasing varied grain structure and residual stress.

Wang et al. [10] observed varying grain structure with an Inconel 625 single bead wall and Li et al. [11] observed varying grain structure with a Titanium alloy single bead wall. AM components are often anisotropic due to the inherent effects of the thermal cycling of a component during the deposition process [10]. Under extreme circumstances, a deposited weld bead can be re-melted over three times [1,12]. This remelting causes large, long grain structure perpendicular to the deposition layer planes in the deposition which can be seen in an investigation of interfacial features [13]. Li et al. [11] and Akerfeldt et al. [14] noted the tensile strength of the deposited material was greater perpendicular to the grain growth indicating more grain boundaries equates to higher ultimate tensile strength.

Increased thermal gradients also increase residual stress as Dandari et al. [15] evaluated while varying dwell time for 6Al-4V Titanium double bead walls; when cooling time was increased between bead depositions, the build plate warping increased indicating increased residual stress [15]. This residual stress is due to the thermal cycling of the AM process [16]. Thermal energy is applied locally at the deposition site, causing the substrate to expand, then the system cools, causing the hot material to contract, creating local stress [17].

Component design and intended use will dictate the desired component material properties and manufacturing process. Some components' grain structure might not be critical; however, fast manufacturing times are required which could benefit from applied cooling during deposition. A different component could require more uniform grain structure which would require the component to be manufactured at a constant temperature and it would not require active cooling. The thermal response of each of these components could be simulated in order to more quickly progress the deposition parameter development and applied cooling strategies.

AM components not only require certain grain structures, but also a specified outer surface roughness. Some AM components require high-quality surface finishes which cannot be achieved only through WAAM [16]. WAAM components can be post-processed by finish-machining the component through subtractive means such as with a computer numeric control (CNC) or ground in order to achieve high dimensional tolerances and surface finish [18]. CNC machines that include subtractive and additive capability are called Hybrid machines [19]. Native subtractive machine tools can also be retrofitted with AM systems which can include metal inert gas (MIG) welders and tungsten inert gas (TIG) welders. Machine tool manufacturers are now developing commercial hybrid systems as well [18]. The integrated hybrid systems allow for interleaving additive and subtractive processes which allows for increased component complexity with more simple tool paths and tooling [20].

Many AM and hybrid systems have deposition rates which exceed the thermal energy dissipation rates, so dwell times are incorporated in the deposition program in order to prevent thermal structural failure by increasing thermal energy dissipation time. The dwell times are often conservatively chosen and determined experimentally which decreases time and material efficiency. In situ monitoring would be a more time-effective way to determine dwell time by continuing deposition when the maximum temperature of the component has cooled to the desired interpass temperature [21]. In situ monitoring integration can be expensive and complex due to the thermal monitoring equipment and machine integration. However, the ability to analytically determine dwell time which is related to maximum interpass temperature can help to further WAAM efficiency. Due to the large amount of boundary variables, a finite element analysis (FEA) model can be used to predict the thermal response of a WAAM component [22]. This FEA model can be developed for a specific deposition system verified with physical control samples that are thermally monitored throughout the deposition process [23]. Once an accurate model

is developed, varied deposition parameters can be tested in order to predict the thermal response of the theoretical system. One application for an FEA model of a WAAM component is the evaluation of the effectiveness of various cooling methods.

Active cooling has been proven to decrease dwell time while retaining comparable part quality [6–9]. Various build plate cooling methods have not been evaluated which focus on differing thermal outcomes ranging from maximum cooling to consistent, higher temperatures. This paper evaluates the thermal response for non-integral build plate cooling, integral build plate cooling, and passive cooling methods which are hypothesized to have differing thermal responses and could have differing efficacy applications. Each cooling method was hypothesized to increase the cooling rate as described by Fourier's Law: increasing the temperature differential between the deposition site and the build plate by decreasing the build plate temperature will increase thermal energy dissipation by conduction energy heat transfer [24]. The differing thermal responses will affect the interpass temperature, residual stress, and grain structure of the manufactured component. Non-integral build plate cooling compared to conventional deposition processing without cooling was analyzed in this investigation with physical experiments which were used to develop the FEA model. The thermal response of integral build plate cooling, and passive cooling with a tall build plate and a wide build plate were analyzed using the developed FEA model. The deposition system used, analysis process, and results of the analysis will be explained later in this paper.

2. MATERIALS AND METHOD

This investigation was performed to determine how differing cooling strategies would affect the thermal response of a WAAM component. A 50.7 mm square was deposited 50 mm tall on build plate with and without conduction cooling. A 3-axis retrofit CNC machine was used to deposit the geometry and the build plate temperature was monitored with bolt-on thermocouples. The manufactured component thermal response was used to develop and verify the FEA model. Then, the same additive geometry was modeled in FEA with no build plate cooling, non-integral build plate cooling, integral build plate cooling, over-sized tall build plate, and over-sized wide build plate to evaluate the thermal response during the additive process. The deposited component tool paths and materials were kept constant for each sample while the dwell time and build plate conditions were varied.

A 3-axis Cincinnati Dart CNC machine was used to position the deposition head along the programmed tool paths which were developed using a slicer [25]. A double bead, 50.7 mm square, was deposited 50 mm tall was the geometry evaluated in this investigation as seen in Figure 1. The conventional non-cooled experiment and the bottom conduction cooled experiment build plates were 6.35 mm thick, 108 mm square mild steel plates.

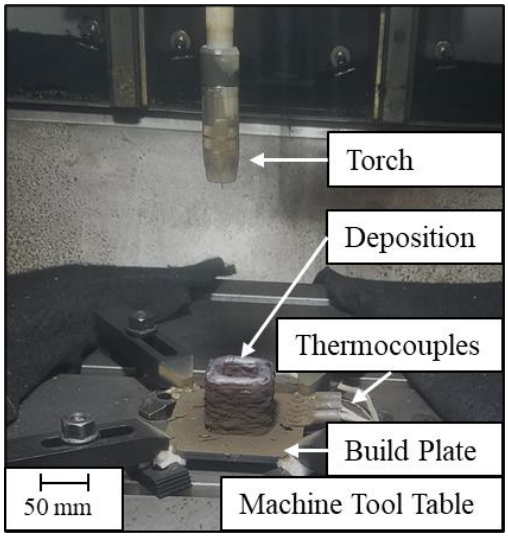

FIGURE 1: HYBRID MACHINE TOOL SETUP USED DURING THE DEPOSITION OF THE COMPONENTS, INCLUDING THE THERMOCOUPLES MOUNTED ON THE BUILD PLATE.

A Lincoln Electric S500 PowerWave Advanced Process Welder was used with a metal inert gas (MIG) torch as the additive head which was mounted co-axially to the machine tool spindle. The torch used can be seen in the top of Figure 1. A wire feed rate of 10.4 m/min was used with 1.1 mm ER70S-6 feedstock wire and pure argon as the shielding gas. The RapidArc welding mode was used for the high-output capability of the S500 welder where the current and voltage averaged 233.1A and 23.6V respectively.

The temperatures of the build plate were monitored using 4 bolt-on type K thermocouples. Three thermocouples were bolted to the build plate along one edge from the middle of one edge, 20 mm apart to 40 mm from the middle, 7.6 mm from the edge. The chosen locations were expected to provide an adequate temperature distribution representative of the entire build plate since the build plate is symmetric in the horizontal and vertical directions. The fourth thermocouple was mounted in the middle of a second edge since the middle of the build plate was expected to experience the highest temperatures and was most likely to thermally fail. The thermocouple mounted in the middle of the build plate was labeled as TC1 where TC2 was mounted 20 mm from the middle and TC3 was mounted 40 mm from the middle. TC4 was mounted in the middle of the second edge along the build plate.

Six samples with two differing build plate cooling conditions were manufactured. Three samples with no build plate cooling classified as a conventional deposition strategy were deposited with dwell times of t_C = 60, 45, and 30 seconds. Three samples with bottom build plate conduction cooling were deposited with dwell times of t_B = 60, 30, and 15 seconds.

ANSYS with the Additive Manufacturing add-in was used to model the thermal response of all of the experiments presented in this article. The add-in models a powder bed type additive process where a controlled thickness of material is perfectly

melted at a determined temperature with a selected scan speed and hatch spacing. The modeled process is specified as direct energy deposition (DED) which includes convection and radiation on the sides of the deposition along with the top. The boundary conditions, such as the convection coefficient, thermal conductivity, and pre-heat temperature are specified by the user.

The boundary conditions used in this study include the convection coefficient, thermal conductivity, feed stock melting temperature, and pre-heat temperature. The values used can be seen in Table 1.

TABLE 1: MODEL BOUNDARY CONDITIONS

Parameter	Value	Unit
Melting temperature	6,000	C
Pre-heat temperature	22	C
Convection [23]	25	W/m^2-K
Scan speed	0.00677	m/s
Hatch spacing	0.0075	m
Steel thermal conductivity [21]	51.9	W/m^2-K
Copper contact thermal conductivity *	525	W/m^2-K
Steel contact thermal conductivity *	8,000	W/m^2-K

*Values determined during model refinement

The melting temperature was chosen from the value of the average center temperature of a welding arc [26]. The preheat temperature was chosen as room temperature. The convection coefficient was chosen as the widely accepted highest values of natural convection [27]. The copper and steel interfacial conductivities were determined during the development of the model. Each boundary condition presented was kept constant throughout all simulations evaluated in this investigation.

The mesh size for each component of the model was determined. Each solid, such as the deposition model, build plate, heat exchangers, and the machine tool table, were modeled as a separate solid. A mesh convergence evaluation was performed and the mesh edge sizes are given in Table 2.

TABLE 2: MODEL MESH EDGE SIZES

Parameter	Value	Unit
Build height	2.31	mm
Build width	5	mm
Build plate	15	mm
Heat exchangers	15	mm
Table	20	mm

The conventional deposition was modeled as the deposition geometry bonded to the build plate with a rough interface of 8,000 W/m^2-K interface thermal conductivity. The build plate bolted on top of steel isolation pads in the actual deposition was modeled with 6.35 mm tall right triangular pads with 12.7 mm side lengths on each corner of the build plate as can be seen in Figure 4a.

The non-integral cooled deposition was modeled as the deposition geometry bonded to the build plate with a rough interface of 525 W/m^2-K interface thermal conductivity between the build plate and the copper heat exchangers. The heat exchangers were modeled as a constant temperature of 5 C which was the average temperature of the inlet water during the deposition process.

The model was developed by setting the known values of the melting temperature, convection, pre-heat temperature, scan speed, hatch spacing, layer height, and material thermal conductivities. The contact thermal conductivities were then determined in order to minimize the error between the model temperatures and the actual deposition temperatures recorded at the thermocouple locations.

Five total conditions were evaluated using FEA; two conditions were the same conditions as the actual samples performed and three new conditions were modeled. The two conditions that were the same as the actual samples included a 6.35 mm thick build plate without cooling and with non-integral build plate cooling. The three new build plate conditions that were modeled and evaluated were of direct build plate cooling with integral cooling passages and passive cooling with a tall and a wide build plate. The abbreviations and dwell times can be seen in Table 3. The oversized mild steel build plate dimensions were chosen such that the total mass was 13.2 kg which is capable of absorbing 1,920 kJ of energy with a change in temperature of 300 C. 1,920 kJ was the amount of energy removed from the t_C = 15 s sample by the conduction cooling system calculated from the temperature difference between the inlet and outlet water temperatures along with the flow rate.

TABLE 3: COOLING METHODS WITH DWELL TIMES

Cooling Method	Dwell Time [s]
Conventional – no cooling	t_C = 60, 30, 20
Non-integral– heat exchangers	t_N = 60, 30, 20
Integral– integral cooling channels	t_I = 60, 30, 20
Tall build plate – passive cooling	t_T = 60, 30, 20
Wide build plate – passive cooling	t_W = 60, 30, 20

The thermal response of an integral build plate was evaluated. The directly cooled build plate was modeled as a 108 mm square build plate, 31.75 mm thick with 18.26 mm inlet and outlet ports and three 14.68 mm perpendicularly drilled cooling channels as can be seen in Figure 2. The channel surfaces were set at a constant temperature of 5 C within the model. The directly cooled build plate dwell times are be represented by t_I = 20 s.

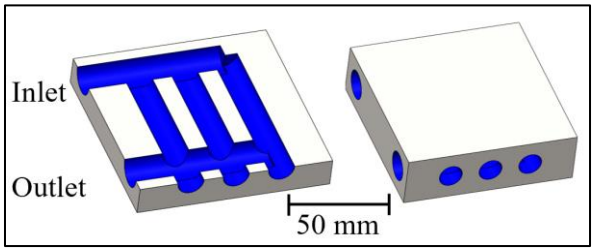

FIGURE 2: INTEGRAL BUILD PLATE COOLING CHANNELS

The thermal response of an oversized, tall build plate was evaluated. The build plate was 139.7 mm in diameter with a length of 106.68 mm. It was hypothesized that the minimal exposed surface area versus the increased mass would isolate the

effect of energy absorption in the mass of the build plate material. The tall build plate dwell times will be represented by t_T = 20 s.

The thermal response of an oversized, wide build plate was evaluated. The build plate was 203.2 mm wide, 635 mm long, and 12.7 mm thick. It was hypothesized the wide build plate could absorb energy and dissipate energy through conduction more effectively than the tall build plate. The wide build plate dwell times will be represented by t_W = 20 s.

3. RESULTS AND DISCUSSION

Six samples were deposited and their thermal responses were monitored. Three conventional samples were deposited without cooling and three samples were deposited with non-integral build plate cooling. Each sample was then modeled in FEA and the difference in the thermal response can be seen in Figure 3. The model temperatures represented by the dashed lines are compared to the actual deposition temperatures as seen in Figure 3.

The model accuracy was verified and can be compared to the actual depositions' thermal response in Figure 3. The red dashed lines represent the maximum interpass temperature before the next layer was deposited. This temperature was not able to be verified due to the limitations of the available non-contact temperature measuring equipment. The cooled build plate temperature error ranged from 2-35% or 2.44-38.13 C. The conventionally deposited sample model error ranged from 23-68% or 94.52-148.88 C. The increased difference between the conventionally deposited model from the actual sample could be accounted for by the convection coefficient chosen for the model. The maximum value for natural convection has been determined to be 25 W/m^2-K [27]. However, due to the high surface temperatures of the component during the deposition process, it is probable that local convection was higher than 25 W/m^2-K due to the high temperatures which could have been as high as 1,000 C for more than a few seconds. A more representative convection coefficient for the deposition geometry during the deposition process would be 55 W/m^2-K. At 55 W/m^2-K, the model build plate varied from the actual build plate temperature by 3.2% or 6.34 C for the t_C = 60 s sample. The cooled sample error was less at the 25 W/m^2-K value due to the conduction cooling of the heat exchangers dissipating more thermal energy than through convection causing less error due to the convection coefficient difference.

The simulations analyzed provide increased understanding of the thermal response of varying build plate cooling conditions and interpass temperature. The hypothesis was concluded to be correct from the simulation results. The conventional deposition strategy had the highest interpass temperature while the directly cooled build plate had the lowest interpass temperature. The passive cooling strategies has a lower, more consistent thermal response as compared to the conventional deposition strategy.

Five different build plate conditions were modeled with three different dwell times. Three dwell times for each sample

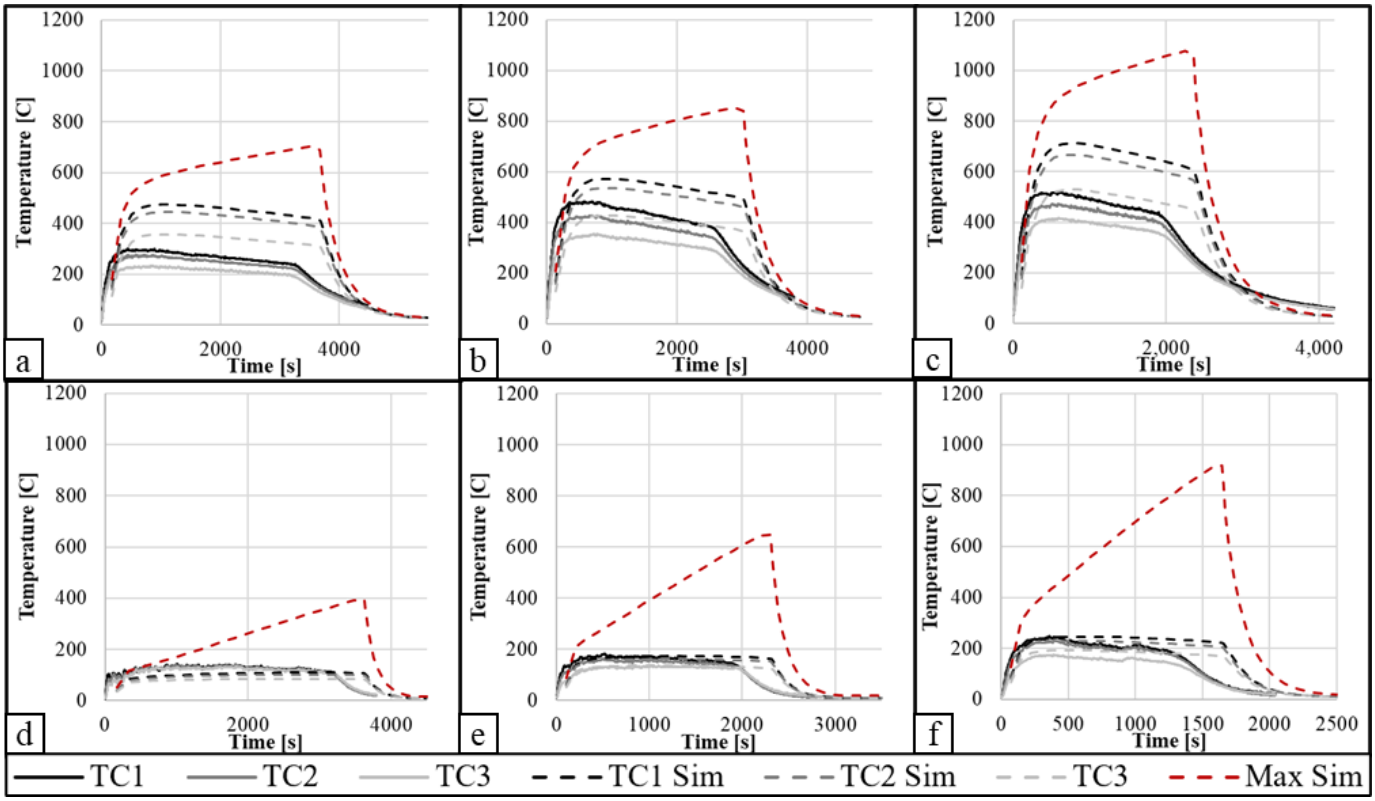

FIGURE 3: SAMPLE TEMPERATURES REPRESENTED BY THE SOLID LINES VERSUS THE SIMULATION TEMPERATURES REPRESENTED BY THE DASHED LINES OF CONVENTIONAL WAAM COMPONENTS (a) t_C = 60 s, (b) t_C = 45 s AND (c) t_C = 30 s AND BOTTOM BUILD PLATE CONDUCITON COOLING OF WAAM COMPONENTS WITH (d) t_N = 60 s, (e) t_N = 30 s AND (f) t_N = 15 s

were evaluated: 60, 30, and 20 seconds between each deposited bead, or 120, 60, and 40 seconds between each layer. The five build plate conditions were as follows:

1. Conventional sample with a 6.35 mm thick build plate without cooling
2. Non-integral cooled build plate sample with a 6.35 mm thick build plate and copper heat exchangers as the cooling method
3. Integral cooled sample with drilled cooling channels within the build plate
4. Tall build plate with a diameter of 139.7 mm and height of 106.68 mm
5. Wide build plate 203.2 mm wide, 635 mm long, and 12.7 mm thick.

Each sample was modeled with the given boundary conditions and mesh dimensions that were described in the previous section. The results of the model can be seen in Figure 4. The temperatures for each sample were recorded at the conclusion of the deposition process which was determined to be an adequate representation of the thermal response of each varying build plate condition. Figure 4 displays the thermal distribution at the conclusion of the deposition process of the 20 second dwell for each sample evaluated with varying build plate conditions. The minimum and maximum temperatures are displayed in blue and red at the bottom of each subfigure, respectively. Figure 4a represents the conventional deposition where no cooling was applied to the 6.35 mm thick build plate. Figure 4b represents the non-integral cooled build plate where the geometry was deposited on a 6.35 mm thick build plate that was cooled with water cooled copper heat exchangers mounted to the bottom of the build plate. Figure 4c represents the integral cooled build plate with integral cooling channels. Figure 4d represents the tall build plate with no applied active cooling. Figure 4e represents the wide build plate with no applied active cooling.

Figure 5 provides the maximum and build plate temperatures for the models at the conclusion of the deposition process, after the specified dwell time. The t_N = 20 s sample build plate temperature was 3.6 times cooler than the t_C = 20 s sample build plate. By only implementing non-integral conduction cooling with re-usable heat exchangers, the maximum interpass temperature is kept 62 degrees C and 209 degrees C lower than the tall and wide over-sized build plates respectively as can be seen in Figure 5. The heat exchangers are a low-cost system for effectively decreasing build plate and interpass temperature. By decreasing interpass temperature, dwell time can be decreased in order to increase the deposition rate with comparable part quality.

The integral build plate cooling method had the lowest temperature response of all of the build plate cooling strategies. The t_I build plate temperatures only varied from 5.47-15.61 C for t_I = 60 s TC3 and t_I = 20 s TC1 respectively. These low build plate temperatures enable the model to have the lowest interpass temperature of all of the methods evaluated in this investigation. This cooling strategy has the lowest temperatures since the cooled working fluid is in direct contact with the build plate material eliminating the contact resistance present in the conduction cooled strategy. However, the low build plate temperatures could inhibit proper wetting of the weld bead with the substrate. The low temperature of the build plate quickly absorbs the thermal energy from the weld bead, quickly solidifying the weld bead. Fast weld bead solidification could be similar to conditions when insufficient thermal energy is used to during the deposition process and improper bonding occurs [28].

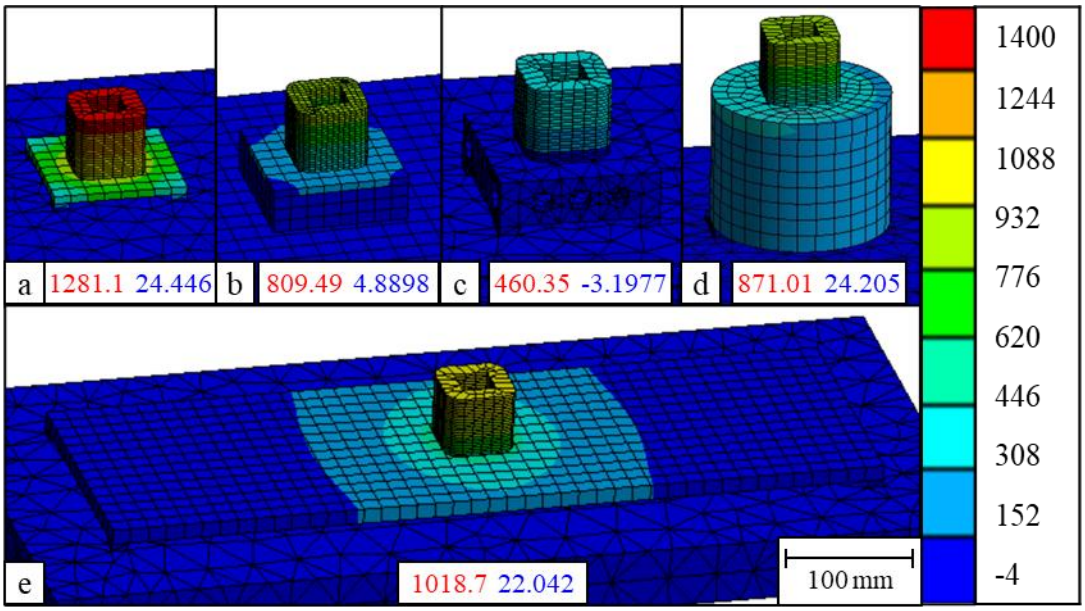

FIGURE 4: THERMAL RESPONSE AT THE CONCLUSION OF THE DEPOSITION PROCESS FOR EACH 20 SECOND DWELL SIMULATION OF WAAM COMPONENTS WITH VARYING BUILD PLATE BOUNDARY CONDITIONS WHERE **(a)** t_C = 20 s, (b) t_N = 20 s, (c) t_I = 20 s, (d) t_T = 20 s, AND (e) t_W = 20 s.

Inadequate weld wetting could occur, causing failure of the manufactured component.

The tall build plate temperature had a slower rise time and local temperatures ranged from 198.05 – 328.41 for the t_T = 60 s TC3 and t_T = 20 s TC1 samples, respectively. The tall build plate was on average cooler than the wide build plate by 42 C between the 60 second dwell samples as comparted to 106 C with the 20 second dwell samples. The tall build plate has a larger cross-sectional area for the thermal energy to conduct through the build plate and shorter distance from the deposition site to the furthest point on the build plate as compared to the wide build plate supporting why the tall build plate temperatures are lower than the wide build plate.

The wide build plate temperatures were higher than the tall build plate due to the distance over which the thermal energy had to travel in order to be absorbed by the total mass of the build plate. The temperature distribution for the tall build plate in Figure 4d is more uniform throughout the build plate mass as compared to the wide build plate in Figure 4e indicating the energy was more uniformly absorbed by the tall build plate. This evaluation indicates using the build plate mass to regulate temperature could be more effective than increased build plate surface area.

Each build plate condition had differing thermal responses which could be applied effectively for different component requirements. Conventional, cooled, and oversized build plates each have various advantages and disadvantages depending on the application. Various advantages and disadvantages of each build plate condition are presented.

The benefits and disadvantages of an oversized build plate are situation dependent. An oversized, tall build plate could be used when excess material is available for depositions and slow cool down of the component is desired. The tall build plate could be used for depositions requiring more uniform, larger grain structure where the build plate mass is pre-heated and the deposition is performed. Due to the increased mass of the build plate, the energy is stored over a longer period of time and the cool down time is increased as compared to thin build plates. However, this strategy increases the height of the deposition start point, decreasing the available build height of the deposition machine by the build plate height. Depending on the available work volume, the tall build plate might be effective.

Using heat exchangers to increase AM build efficiency depends on the application. The heat exchanger strategy could be effective when the scale of the manufactured component varies since the heat exchangers can be scaled. The heat exchanger concept is also not limited to use on WAAM systems; they can be mounted to many AM component build plates as long as the cooling system is properly sealed. The heat exchangers can also be re-used whereas the oversized build plate reuse would be limited or time prohibitive. The reusability of the heat exchangers is more environmentally friendly as compared to a consumable cooling strategy, such as the directly cooled build plate.

The integral cooled build plate strategy had the lowest part temperatures; however, each drilled build plate would have to be manufactured separately for every deposition since the part removal process could damage the cooling channels of the build plate, further increasing the manufacturing time for a cooled component. However, the integral cooling strategy could be useful for large, low thermal conductivity components when increasing heat flow is critical. Also, by integrating the cooling channels into the build plate, the rigidity of the system is increased as compared to a large build plate or attached heat exchangers. The drilled build plate can be directly clamped to the hybrid system if additive and subtractive processes are conducted in a single machine tool.

Each build plate cooling strategy had a unique thermal response, but the effectiveness of each strategy is application dependent. Non-integral build plate cooling reduced the interpass temperature for the t_N = 20 s by 36% as compared to the t_C = 20 s strategy. Integral build plate cooling reduced the

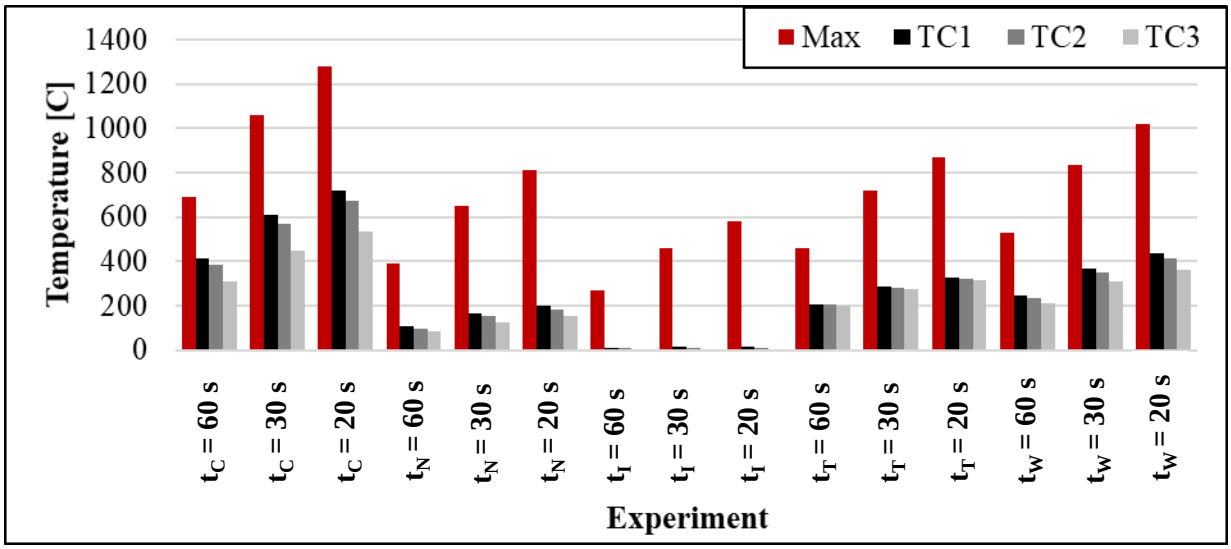

FIGURE 5: MODEL TEMPERATURES AT THE CONCLUSION OF THE DEPOSITION PROCESS FOR EACH BUILD PLATE CONDITION.

interpass temperature for the t_I = 20 s by 32% as compared to the t_N = 20 s strategy. The tall build plate reduced the interpass temperature for the t_T = 20 s by 32% as compared to the t_C = 20 s strategy. The wide build plate reduced the interpass temperature for the t_W = 20 s by 20% as compared to the t_C = 20 s strategy. Material thermal conductivity will impact the effectiveness of each cooling strategy as well.

4. CONCLUSIONS

The present study investigated the thermal response of various cooling strategies for a WAAM component. The cooling response of each scenario was evaluated with an accurate FEA model of the system that was designed and verified with multiple depositions. By understanding the effectiveness of each cooling method, future experiments can implement the strategy that best suits the need.

It was determined that each build plate cooling strategy effectiveness is dependent on the application and material properties of the build plate and feed stock. If maximum cooling is desired, direct build plate cooling should be used. Integral build plate cooling was shown to decrease the interpass temperature by 55% and build plate temperature by 96% compared to the t_C = 20 s strategy. If no liquid coolant can be used in the build volume, a large, tall build plate could be useful. The tall build plate reduced the interpass temperature for the t_T = 20 s by 32% as compared to the t_C = 20 s strategy. If constant, raised build plate temperature is desired in order to achieve more consistent bead geometry and slower cool down time, a tall, pre-heated build plate could be effective. If component size is constantly changing and quick changeover time is desired with little material waste, the heat exchanger strategy would be effective. Non-integral build plate cooling through the implementation of heat exchangers reduced the interpass temperature for the t_N = 20 s by 36% as compared to the t_C = 20 s strategy.

Build plate cooling can be implemented through non-integral cooling of a thin build plate, integral cooling the build plate with integrated cooling channels, or passively cooling the component with an oversized build plate that can absorb some of the thermal energy. Each strategy evaluated significantly decreased the build plate and interpass temperature of the WAAM component.

ACKNOWLEDGEMENTS

This work is funded by the Department of Energy DE-EE0008303 with the support of Oak Ridge National Laboratory.

REFERENCES

[1] Dinovitzer, M., Chen, X., Laliberte, J., Huang, X., and Frei, H., 2019, “Effect of Wire and Arc Additive Manufacturing (WAAM) Process Parameters on Bead Geometry and Microstructure,” Addit. Manuf., **26**, pp. 138–146.

[2] Froes, F. H., and Dutta, B., 2014, “The Additive Manufacturing (AM) of Titanium Alloys,” Adv. Mater. Res., **1019**, pp. 19–25.

[3] Cunningham, C. R., Flynn, J. M., Shokrani, A., Dhokia, V., and Newman, S. T., 2018, “Invited Review Article: Strategies and Processes for High Quality Wire Arc Additive Manufacturing,” Addit. Manuf., **22**, pp. 672–686.

[4] Carter, W., Masuo, C., Nycz, A., Noakes, M., and Vaughan, D., 2019, “Thermal Process Monitoring for Wire-Arc Additive Manufacturing Using IR Cameras,” Austin, Texas, United States of America, p. 6.

[5] Wu, B., Ding, D., Pan, Z., Cuiuri, D., Li, H., Han, J., and Fei, Z., 2017, “Effects of Heat Accumulation on the Arc Characteristics and Metal Transfer Behavior in Wire Arc Additive Manufacturing of Ti6Al4V,” J. Mater. Process. Technol., **250**, pp. 304–312.

[6] Fang Li, Shujun Chen, Junbiao Shi, Yun Zhao, and Hongyu Tian, 2018, “Thermoelectric Cooling-Aided Bead Geometry Regulation in Wire and Arc-Based Additive Manufacturing of Thin-Walled Structures,” Appl. Sci., **8**(2), p. 207.

[7] Wang, B., Yang, G., Zhou, S., Cui, C., and Qin, L., 2020, “Effects of On-Line Vortex Cooling on the Microstructure and Mechanical Properties of Wire Arc Additively Manufactured Al-Mg Alloy,” Metals, **10**(8), p. 1004.

[8] Koike, R., Pagano, L., Kakinuma, Y., Oda, Y., and Kondo, M., 2019, “Stabilization of Metal Structure Formation in Directed Energy Deposition by Applying a Coolant System,” Procedia Manuf., **40**, pp. 38–44.

[9] Kozamernik, N., Bračun, D., and Klobčar, D., 2020, “WAAM System with Interpass Temperature Control and Forced Cooling for Near-Net-Shape Printing of Small Metal Components,” Int. J. Adv. Manuf. Technol., **110**(7–8), pp. 1955–1968.

[10] Wang, J. F., Sun, Q. J., Wang, H., Liu, J. P., and Feng, J. C., 2016, “Effect of Location on Microstructure and Mechanical Properties of Additive Layer Manufactured Inconel 625 Using Gas Tungsten Arc Welding,” Mater. Sci. Eng. A, **676**, pp. 395–405.

[11] Li, Z., Liu, C., Xu, T., Ji, L., Wang, D., Lu, J., Ma, S., and Fan, H., 2019, “Reducing Arc Heat Input and Obtaining Equiaxed Grains by Hot-Wire Method during Arc Additive Manufacturing Titanium Alloy,” Mater. Sci. Eng. A, **742**, pp. 287–294.

[12] Chekir, N., Tian, Y., Gauvin, R., Brodusch, N., Sixsmith, J. J., and Brochu, M., 2018, “Laser Wire Deposition of Thick Ti-6Al-4V Buildups: Heat Transfer Model, Microstructure, and Mechanical Properties Evaluations,” Metall. Mater. Trans. A, **49**(12), pp. 6490–6508.

[13] Feldhausen, T., Kannan, R., Raghavan, N., Saleeby, K., Kurfess, T., and Nandwana, P., 2021, “Investigation of Interfacial Structures for Hybrid Manufacturing,” Mater. Lett., p. 131040.

[14] Åkerfeldt, P., Antti, M.-L., and Pederson, R., 2016, “Influence of Microstructure on Mechanical Properties of Laser Metal Wire-Deposited Ti-6Al-4V,” Mater. Sci. Eng. A, **674**, pp. 428–437.

[15] Bandari, Y. K., Lee, Y. S., Nandwana, P., Richardson, B. S., Adediran, A. I., and Love, L. J., 2018, “Effect of Inter-Layer

Cooling Time on Distortion and Mechanical Properties in Metal Additive Manufacturing," *Proceedings of the 29th Annual International Solid Freeform Fabrication Symposium-An Additive Manufacturing Conference-2018*, Austin, Texas, United States of America, p. 13.

[16] Dávila, J. L., Neto, P. I., Noritomi, P. Y., Coelho, R. T., and da Silva, J. V. L., 2020, "Hybrid Manufacturing: A Review of the Synergy between Directed Energy Deposition and Subtractive Processes," Int. J. Adv. Manuf. Technol., **110**(11–12), pp. 3377–3390.

[17] Li, C., Liu, Z. Y., Fang, X. Y., and Guo, Y. B., 2018, "Residual Stress in Metal Additive Manufacturing," Procedia CIRP, **71**, pp. 348–353.

[18] Flynn, J. M., Shokrani, A., Newman, S. T., and Dhokia, V., 2016, "Hybrid Additive and Subtractive Machine Tools – Research and Industrial Developments," Int. J. Mach. Tools Manuf., **101**, pp. 79–101.

[19] Cortina, M., Arrizubieta, J., Ruiz, J., Ukar, E., and Lamikiz, A., 2018, "Latest Developments in Industrial Hybrid Machine Tools That Combine Additive and Subtractive Operations," Materials, **11**(12), p. 2583.

[20] Feldhausen, T., Raghavan, N., Saleeby, K., Love, L., and Kurfess, T., 2021, "Mechanical Properties and Microstructure of 316L Stainless Steel Produced by Hybrid Manufacturing," J. Mater. Process. Technol., **290**, p. 116970.

[21] Feldhausen, T., Saleeby, K., and Kurfess, T., 2021, "Spinning the Digital Thread with Hybrid Manufacturing," Manuf. Lett., p. S2213846321000249.

[22] Heinrich, L., Kurfess, T. R., Feldhausen, T., Saleeby, K. S., and Saldana, C., 2021, "PREDICTION OF THERMAL CONDITIONS OF DED WITH FEA METAL ADDITIVE SIMULATION," p. 9.

[23] Heinrich, L., 2022, "Build Plate Conduction Cooling for Thermal Management of Wire Arc Additive Manufactured Components," Master's Thesis, Georgia Institute of Technology.

[24] Callister, W. D., Jr., and Rethwisch, D. G., 2010, *Materials Science and Engineering*, John Wiley and Sons, Inc.

[25] 2019, *ORNL Slicer Engine*, Oak Ridge National Laboratory.

[26] Doshi, S., Jani, D. B., Gohil, A. V., and Patel, C. M., 2021, "Progress in the Arc Plasma Temperature Measurement and Its Finite Element Analysis in Pulsed MIG Welding Process," Mater. Today Proc., **38**, pp. 2745–2750.

[27] Incropera, F. P., Dewitt, D. P., Lavine, A. S., and Bergman, T. L., 2011, *Introduction to Heat Transfer*, John Wiley and Sons, Inc.

[28] Lin, Z., Ya, W., Subramanian, V. V., Goulas, C., di Castri, B., Hermans, M. J. M., and Pathiraj, B., 2020, "Deposition of Stellite 6 Alloy on Steel Substrates Using Wire and Arc Additive Manufacturing," Int. J. Adv. Manuf. Technol., **111**(1–2), pp. 411–426.